Symmetry rules and strain/order-parameter relationships for coupling between octahedral tilting and cooperative Jahn–Teller transitions in ABX_3 perovskites. II. Application

Michael A. Carpenter[a]* **and Christopher J. Howard**[a,b]

[a]Department of Earth Sciences, University of Cambridge, Downing Street, Cambridge CB2 3EQ, England, and [b]School of Engineering, University of Newcastle, NSW 2308, Australia

Correspondence e-mail: mc43@esc.cam.ac.uk

The structural evolution of selected perovskites containing Jahn–Teller cations has been investigated in the light of a formal analysis of symmetry hierarchies for phase transitions driven by octahedral tilting and Jahn–Teller cooperative distortions. General expressions derived from the strain/order-parameter coupling relationships allowed by symmetry are combined with observed changes in lattice parameters to reveal details of order-parameter evolution and coupling. $LuVO_3$, $YbVO_3$, YVO_3 and $CeVO_3$ are representative of systems which develop Jahn–Teller ordering schemes associated with irreducible representations M_2^+ and R_3^+ of the space group $Pm\bar{3}m$. Tilting of their octahedra is associated with M_3^+ and R_4^+. The $Pnma$ ($M_3^+ + R_4^+$ tilting) $\leftrightarrow$ $P2_1/a$ ($M_3^+ + R_4^+$ tilting, R_3^+ Jahn–Teller order) transition below room temperature is close to second order in character. Shear strains which depend primarily on tilt angles show little variation, implying that there is only weak coupling between the tilting and Jahn–Teller order parameters. The subsequent $P2_1/a \leftrightarrow Pnma$ ($M_3^+ + R_4^+$ tilting, M_2^+ Jahn–Teller order) is first order in character, and involves either a reduction in the R_4^+ tilt angle or a change in the strength of tilt/Jahn–Teller order-parameter coupling. In $LaMnO_3$, the isosymmetric $Pnma$ ($M_3^+ + R_4^+$ tilting) $\leftrightarrow$ $Pnma$ ($M_3^+ + R_4^+$ tilting, M_2^+ Jahn–Teller order) transition can be described in terms of a classical first-order transition conforming to a 246 Landau expansion with negative fourth-order coefficients. Strain evolution in Ba-doped samples suggests that the transition becomes second order in character and reveals a new strain relaxation mechanism in $LaMnO_3$ which might be understood in terms of local strain heterogeneities due to the disordering of distorted MnO_6 octahedra. Transitions in $PrAlO_3$ and $La_{0.5}Ba_{0.5}CoO_3$ illustrate the transformation behaviour of systems in which the Jahn–Teller ordering scheme is associated with the irreducible representation Γ_3^+. Overall, coupled tilting + Jahn–Teller phase transitions in perovskites conform to mean-field behaviour, consistent with the underlying role of strain in promoting long interaction lengths.

1. Introduction

Perovskites containing Jahn–Teller cations include some highly topical materials. For example, $TbMnO_3$ and $DyMnO_3$ (Kimura *et al.*, 2003; Goto *et al.*, 2004) form part of a group of multiferroic systems which is the subject of intense scrutiny for the combined magnetic and ferroelectric properties which they display. Similarly, $RNiO_3$ (R = La, . . . Lu) perovskites undergo a metal–insulator transition and $LaMnO_3$ provides the end-member for solid-solution series such as $(La,Ca)MnO_3$, $(La,Sr)MnO_3$ which show colossal magnetoresistance (*e.g.* Goodenough, 2004). The properties of interest

research papers

seem to depend on small variations of the basic perovskite structure, but the fact that they arise, characteristically, at discrete structural phase transitions shows that they are due to collective behaviour. As with phase transitions more generally, therefore, the mechanisms of symmetry-breaking processes and the strains which arise from them may play a fundamental role in determining the structure/property relations. In an accompanying paper, Carpenter & Howard (2009) have used group theory and Landau theory to systematize the space groups and possible phase transitions of perovskites which have different combinations of Jahn-Teller distortions and octahedral tilting. The purpose of the present paper is to extend this formal overview to the practical investigation of order-parameter evolution and strain/order-parameter coupling in selected, real systems.

The group-theoretical treatment of Carpenter & Howard (2009) was based on the use of three irreducible representations, Γ_3^+, M_2^+ and R_3^+, of the space group $Pm\bar{3}m$ to represent the three most common Jahn–Teller ordering schemes of ABX_3 perovskites and two, M_3^+ and R_4^+, to represent the different possible tilt systems. Associated with any phase transitions between the possible structure types will be macroscopic spontaneous strain, depending on the precise change in symmetry. General expressions for the relationships between strain and the order-parameter components were also derived using Landau theory. In a number of recent studies (Carpenter, 2007a,b; Carpenter et al., 2001, 2005, 2006; McKnight et al., 2009) it has been found that knowledge of the symmetry properties and strain/order-parameter relationships provides a rigorous formal framework for determining the evolution of perovskites with multiple phase transitions across multicomponent order-parameter space, through the analysis of high-resolution lattice-parameter data. Here, lattice-parameter data from the literature for selected Jahn–Teller perovskites, including LuVO$_3$, YbVO$_3$, YVO$_3$, CeVO$_3$, (La,Ba)MnO$_3$ at small Ba-doping levels, PrAlO$_3$ and La$_{0.5}$Ba$_{0.5}$CoO$_3$, are analysed from the same point of view. In each case there are measurable spontaneous strains ($\gtrsim 0.001$), and the patterns of order-parameter evolution which they reveal are consistent with mean-field behaviour. For LaMnO$_3$ the strain evolution with temperature suggests an unusual strain/order-parameter coupling mechanism in which the Jahn–Teller order parameter causes a renormalization of the coupling coefficient for strain/tilt coupling.

In the following, extensive use is made of the equations given by Carpenter & Howard (2009). §2 contains an analysis of Jahn–Teller + octahedral tilting transitions in vanadate perovskites and §3 deals with manganites. These have M_2^+ and/or R_3^+ as the active representation for the Jahn–Teller ordering, corresponding to different ordering schemes of distorted octahedra. In the literature M_2^+ ordering is more usually described as d-type (equivalent to C-type), in which octahedra in one layer of the structure are overlain by octahedra in the next that have their long axes in the same orientation (see, for example, Okazaki, 1969a,b; Lufaso & Woodward, 2004; Sage et al., 2007). R_3^+, more usually referred to as a-type (or G-type), refers to the ordering scheme in

which octahedra in one layer are overlain in the next layer by octahedra which have their long axes rotated through 90°. In §4 the third ordering scheme, associated with Γ_3^+, is represented by the examples of PrAlO$_3$ and La$_{0.5}$Ba$_{0.5}$CoO$_3$. In this ordering scheme the unique axis of every Jahn–Teller distorted octahedron is aligned in a single direction. The extent of ordering is defined by order-parameter components $q_{1JT}, q_{2JT}, q_{3JT}$ for M_2^+, q_{4JT}, q_{5JT} for R_3^+, and q_{tz}, q_{oz} for Γ_3^+. The extent of octahedral tilting is defined by order-parameter components q_1, q_2, q_3 for M_3^+, and q_4, q_5, q_6 for R_4^+ (Table 1; Carpenter & Howard, 2009).

2. Jahn–Teller + octahedral tilting transitions in RVO$_3$ perovskites

Published lattice parameters and thermal expansion data for LuVO$_3$, YbVO$_3$, YVO$_3$ and CeVO$_3$ are analysed here in light of the symmetry and strain relations set out in Carpenter & Howard (2009). These phases are typical of vanadate perovskites in having tilted octahedra and the space group $Pnma$ at room temperature (Miyasaka et al., 2003; Sage et al., 2007; Martínez-Lope et al., 2008). Below room temperature, they undergo a Jahn–Teller orbital-ordering transition, giving the symmetry change $Pnma \rightarrow P2_1/c$. LuVO$_3$, YbVO$_3$ and YVO$_3$ undergo a further transition, $P2_1/c \rightarrow Pnma$, in which the ordering scheme changes from R_3^+ (a-type) to M_2^+ (d-type). There is also an antiferromagnetic transition. Summaries of this overall behaviour are given by Miyasaka et al. (2003) and Sage et al. (2007). Different space groups have been used to describe the monoclinic structure (e.g. Blake et al., 2001, 2002; Bordet et al., 1993; Muñoz et al., 2003a,b, 2004a,b; Ren et al., 2003; Reehuis et al., 2006, Sage et al., 2007). Here the non-conventional setting $P2_1/a$ ($\gamma \neq 90°$) provides the required order-parameter and orientation relationships, with respect to $Pnma$ for calculation of the spontaneous strains (see Table 1 and Fig. 2 of Carpenter & Howard, 2009).

In $P2_1/a$ crystals the R_3^+ order-parameter components are $q_{4JT} = (\sqrt{3}a_{JT})/2$, $q_{5JT} = -(a_{JT}/2)$ and the non-zero tilt components are $q_2, q_4 = q_6, q_5$. Substituting these into the strain/order-parameter relationships in §3 of Carpenter & Howard (2009) gives tilting and JT contributions to the shear strains as

$$e_{tx} = \frac{-2\left(\lambda_3 q_2^2 - \lambda_4\left(q_4^2 - q_5^2\right)\right) + \lambda_{tR3+} a_{JT}^2}{\frac{1}{2}(C_{11}^o - C_{12}^o)} \quad (1)$$

$$e_{ox} = 0 \quad (2)$$

$$e_4 = \frac{-\lambda_5 q_4^2 - \lambda_{eR3+R4+} a_{JT} q_5}{C_{44}^o} \quad (3)$$

$$e_5 = e_6 = \frac{-\lambda_5 q_5 q_4 + \frac{1}{2}\lambda_{eR3+R4+} a_{JT} q_4}{C_{44}^o}. \quad (4)$$

The volume strain, e_a, becomes

$$e_a = -\left[\frac{\lambda_1 q_2^2 + \lambda_2(2q_4^2 + q_5^2) + \lambda_{aR3+} a_{JT}^2}{\frac{1}{3}\left(C_{11}^o + 2C_{12}^o\right)}\right]. \tag{5}$$

From Table 1 of Carpenter & Howard (2009), there are effectively three possible JT + tilt structures with *Pnma* symmetry. The most likely of these is the one with M_2^+ Jahn–Teller ordering and both M_3^+ and R_4^+ tilts, in which the non-zero order-parameter components are q_{2JT}, q_2 and $q_4 = q_6$. The strain/order-parameter relationships are then

$$e_{tx} = \frac{-2(\lambda_3 q_2^2 - \lambda_4 q_4^2) - 2\lambda_{tM2+} q_{2JT}^2}{\frac{1}{2}\left(C_{11}^o - C_{12}^o\right)} \tag{6}$$

$$e_{ox} = 0 \tag{7}$$

$$e_4 = \frac{-\lambda_5 q_4^2 - \lambda_{eM2+M3+} q_{2JT} q_2}{C_{44}^o} \tag{8}$$

$$e_5 = e_6 = 0 \tag{9}$$

$$e_a = -\left[\frac{\lambda_1 q_2^2 + 2\lambda_2 q_4^2 + \lambda_{aM2+} q_{2JT}^2}{\frac{1}{3}\left(C_{11}^o + 2C_{12}^o\right)}\right]. \tag{10}$$

Values of individual components are derived from the lattice parameters for *Pnma* crystals according to (from Carpenter *et al.*, 2001)

$$e_1 = \frac{\frac{b}{2} - a_o}{a_o} \tag{11}$$

$$e_2 + e_3 = \frac{\frac{a}{\sqrt{2}} - a_o}{a_o} + \frac{\frac{c}{\sqrt{2}} - a_o}{a_o} \tag{12}$$

$$e_4 = \frac{\frac{a}{\sqrt{2}} - a_o}{a_o} - \frac{\frac{c}{\sqrt{2}} - a_o}{a_o}, \tag{13}$$

where a_o is the reference cubic parameter extrapolated from high temperatures. If lattice parameters for the $P2_1/a$ setting of the monoclinic structure are used to calculate the strains, these expressions remain the same except that the a lattice parameter in (11)–(13) is replaced by $a\sin\gamma$ ($\simeq a$ for $\gamma \simeq 90°$) and the additional shear strains are

$$e_5 = e_6 = \frac{1}{\sqrt{2}}\frac{a}{a_o}\cos\gamma \simeq \frac{1}{\sqrt{2}}\cos\gamma. \tag{14}$$

Fig. 1 shows lattice-parameter data for LuVO$_3$, YbVO$_3$, YVO$_3$ and CeVO$_3$ reproduced from Muñoz *et al.* (2003a, 2004a), Marquina *et al.* (2005) and Ren *et al.* (2003), respectively. The data of Marquina *et al.* (2005) for YVO$_3$ were from linear thermal expansion measurements, given with respect to room temperature. Points taken at 5 K intervals from their Fig. 1 have been converted to lattice-parameter values using the room-temperature data of Martínez-Lope *et al.* (2008). Although all four of these vanadate phases passed through the stability field of the monoclinic structure, values of the monoclinic angle were determined only by Ren *et al.* (2003) for CeVO$_3$. This angle is close to 90°, and no serious error is introduced into the strain calculation by assuming $\gamma = 90°$ for
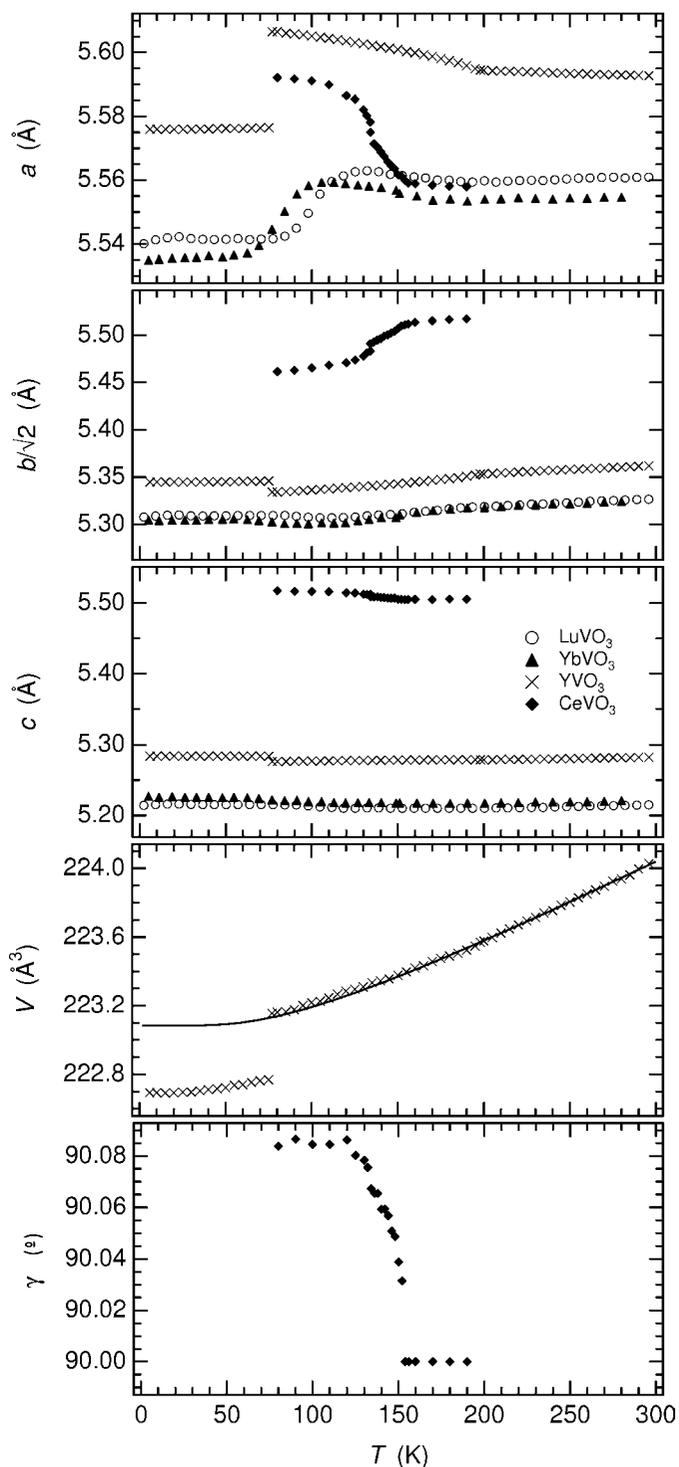
Figure 1
Variations with temperature of lattice parameters for LuVO$_3$ (taken from Muñoz *et al.*, 2004a), YbVO$_3$ (Muñoz *et al.*, 2003a), YVO$_3$ (Marquina *et al.*, 2005) and CeVO$_3$ (Ren *et al.*, 2003). Linear thermal expansion data of Marquina *et al.* (2005) for YVO$_3$ were converted to lattice-parameter values by calibration with the room-temperature data of Martínez-Lope *et al.* (2008). All are given for the *Pnma* and $P2_1/a$ unit-cell settings. The monoclinic angle, γ, was determined only by Ren *et al.* (2003). The curve shown through the unit-cell volume data for YVO$_3$ is a fit of the function $V_o = y_0 + y_1\Theta_{so}\coth(\Theta_{so}/T)$ ($y_0 = 222.44$ Å^3, $y_1 = 0.00503$ Å^3 K^{-1}, $\Theta_{so} = 128.02$ K) to data in the temperature interval 200–300 K (*Pnma*, no JT). It extrapolates through data in the stability field of the $P2_1/a$ structure.
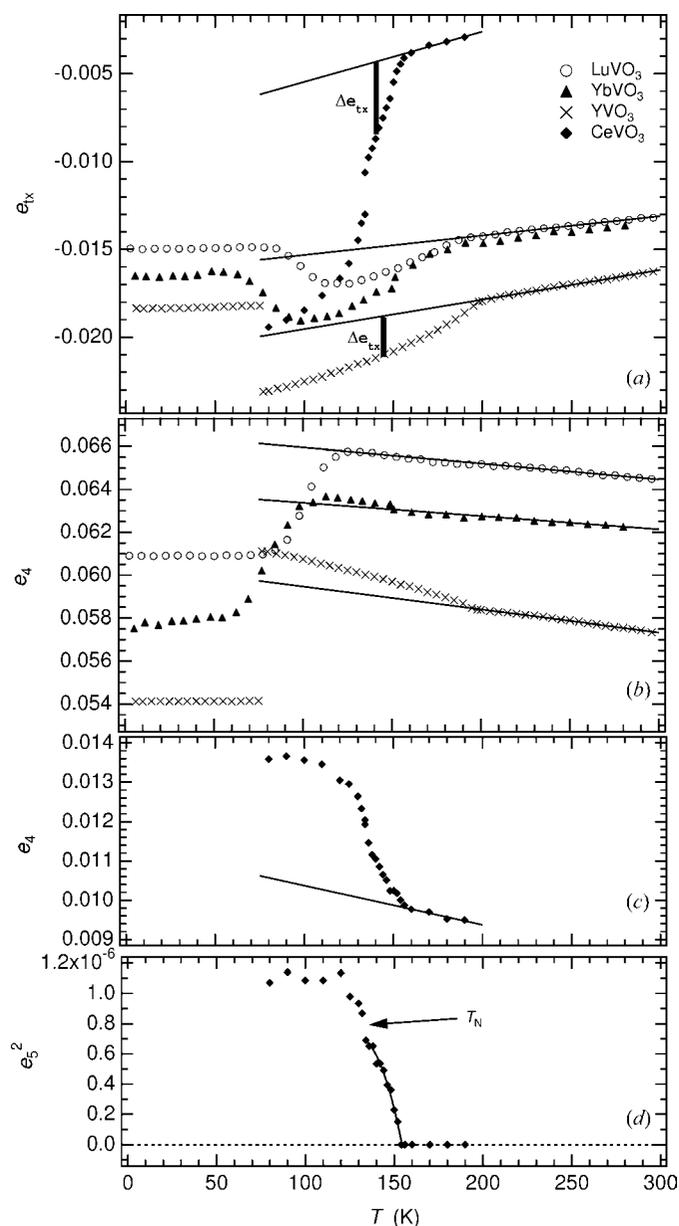
Figure 2
Symmetry-adapted strains calculated from the lattice-parameter data given in Fig. 1. (a)–(c) Straight lines have been fit to data for the *Pnma* phase above the *Pnma* → $P2_1/a$ transition in order to highlight the changes in strain associated with this transition. The magnitude of e_4 is primarily a measure of the R_4^+ tilt angle; it shows no deflection at the *Pnma* → $P2_1/a$ transition of LuVO$_3$ and the largest deflection in CeVO$_3$. The subsequent $P2_1/a$ → *Pnma* transition is first order in character, as shown most clearly at ∼ 77 K in the data for YVO$_3$ derived from linear thermal expansion measurements. The value of e_{tx} is a more sensitive measure of the JT order parameter and the *Pnma* → $P2_1/a$ transition is marked by a change in trend which is slightly non-linear in each of the four vanadates. The Néel temperatures, T_N, of LuVO$_3$, YbVO$_3$, YVO$_3$ and CeVO$_3$ are ∼ 107 K (Muñoz *et al.*, 2004a), ∼ 104 K (Muñoz *et al.*, 2003a), ∼ 116 K (Marquina *et al.*, 2005) and ∼ 134 K (Ren *et al.*, 2003), respectively. Only in the case of CeVO$_3$ is there an obvious change in the trend of symmetry-breaking strains at T_N. (d) e_5^2 is expected to vary as the square of the JT order parameter. Between T_c and T_N it varies almost linearly with temperature, implying close to classical second-order character for the transition. The curve shown through the data is a guide to the eye which emphasizes a slight curvature that could be attributed to the influence of a sixth-order term in the Landau potential.

$e_2 + e_3$ and e_4. Since the data do not extend into the stability field of the cubic phase, it is not possible to determine a_o by extrapolation. Rather, a_o has been approximated as $a_o = (a_c b_c c_c)^{1/3}$, where $a_c = a_{Pnma}/\sqrt{2}$, $b_c = b_{Pnma}/2$ and $c_c = c_{Pnma}/\sqrt{2}$. This approximation also does not introduce serious error into calculated values of the shear strains. Variations of e_{tx}, e_4 and e_5 for LuVO$_3$, YbVO$_3$, YVO$_3$ and CeVO$_3$ are given in Fig. 2.

2.1. Octahedral tilting

Shear strain e_4 provides information relating primarily to q_4 which, in turn, relates to the R_4^+ tilt angle. Combined tilt angles at room temperature are in the range 19–12° (Martínez-Lope *et al.*, 2008). In LuVO$_3$ there is no deflection in the variation of e_4 with temperature at the *Pnma* → $P2_1/a$ transition point (∼ 175 K according to Miyasaka *et al.*, 2003; ∼ 185 K based on the deflection shown by e_{tx} in Fig. 2), suggesting that the already large tilt angles are only weakly influenced, if at all, by the Jahn–Teller ordering. Small changes in e_4 are observed for the other phases, but these are less than ∼ 0.003, even in CeVO$_3$. Additional tilting corresponding to q_5 (allowed under $P2_1/a$ but not under *Pnma* symmetry) is therefore presumably also small. A further, distinct anomaly is visible in all the strains at the Néel temperature of CeVO$_3$ (∼ 134 K; Ren *et al.*, 2003).

The $P2_1/a$ → *Pnma* transition at lower temperatures is necessarily first order in character and occurs with a marked decrease in e_4. This can be understood in terms of a reduction in the R_4^+ tilt angle and/or the change in JT/tilt coupling [*cf.* (3) and (8)]. Apparently continuous variations through the transition temperature shown by LuVO$_3$ and YbVO$_3$ are presumably due to a two-phase coexistence or to some line broadening in the original powder diffraction patterns.

More direct evidence that any changes in octahedral tilt angles associated with the ordering processes are small is provided by the variation of V—O—V bond angles with temperature in YVO$_3$ (Blake *et al.*, 2001, 2002). This angle provides a measure of the total tilt angle of the octahedra (Martínez-Lope *et al.*, 2008). For YVO$_3$ there is no change in trend of the bond angle at the *Pnma* → $P2_1/a$ transition and there is a reduction of less than 0.2% at the $P2_1/a$ → *Pnma* transition (Fig. 8b of Blake *et al.*, 2002).

2.2. Jahn–Teller order parameters

Variations of e_{tx} might provide the most information about the JT order parameters, depending on the extent to which the contributions from $M_3^+(q_2)$ and $R_4^+(q_4)$ tilts cancel each other out [*cf.* (1) and (6)]. If it is assumed that the tilt angles vary very little, the change in e_{tx} due to the *Pnma* → $P2_1/a$ transition, Δe_{tx}, relates essentially to the variation of a_{JT}^2 [see equation (1)]. It is clear from Fig. 2(a) that Δe_{tx} obtained with respect to a linear extrapolation of e_{tx} data from high temperatures would go continuously to zero at the *Pnma* (tilt only) → $P2_1/a$ transition, although not necessarily quite with a linear temperature dependence. The implication is that the JT transition is itself close to being second order in character.

This is confirmed by plots of e_5^2 against temperature (Fig. 2d) and e_5^2 against Δe_{tx} (Fig. 3) for CeVO$_3$, since $e_5 \propto a_{JT}$ for constant q_4 and small q_5 [equation (4)]. It is also notable that in the *Pnma* (+JT) structure, e_{tx} values lie close to values extrapolated from the *Pnma* (no JT) structure at higher temperatures, implying that the coupling coefficient λ_{tM2+} in (6) is small.

Sage *et al.* (2007) found that RVO$_3$ perovskites with R = Tb, Gd, Eu, Sm and Nd can consist of two-phase intergrowths in which one phase has M_2^+ JT order and the second has R_3^+ order. For larger R^{3+} cations there is a first-order transition between the two ordering schemes (Blake *et al.*, 2001, 2002; Miyasaka *et al.*, 2003; Ren *et al.*, 2003; Sage *et al.*, 2007) which, in terms of two JT order parameters, would correspond to the pattern represented by Fig. 6(*e*) or (*f*) of Carpenter & Howard (2009). At temperatures corresponding to the two-phase regions, the relative energies of the JT ordering schemes are finely balanced, providing the most likely scenario for the development of alternative, mixed ordering schemes such as are shown in Table 3 and Fig. 7 of Carpenter & Howard (2009). In this context, it is interesting to note that Sage *et al.* (2007) reported anomalies in the evolution of the lattice parameters of JT structures in the two-phase region.

2.3. Systematics for RVO$_3$ structures

Fig. 4 shows variations of e_{tx} and e_4 as a function of the ionic radius of the R cation in RVO$_3$ perovskites at room temperature, using the lattice-parameter data of Martínez-Lope *et al.* (2008). The tetragonal shear strain remains small in comparison with e_4 at all compositions, as expected for *Pnma* structures, although both are larger in magnitude than observed in CaTiO$_3$ (Carpenter *et al.*, 2001) or SrZrO$_3$ (McKnight *et al.*, 2009). A striking feature is the pseudocubic geometry which develops with increasing radius towards the La^{3+} end-member. In particular, LaVO$_3$ has close to cubic lattice parameters, in spite of having a total tilt angle of $\sim 12°$ (Martínez-Lope *et al.*, 2008) and transition temperatures of
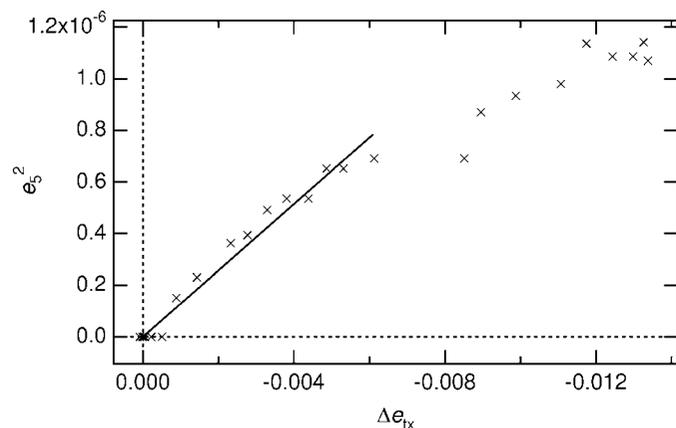
1113 and 1298 K, respectively, for the $R\bar{3}c \leftrightarrow Pnma$ and $Pm\bar{3}m \leftrightarrow R\bar{3}c$ tilting transitions (Zubkov *et al.*, 1980, in Martínez-Lope *et al.*, 2008). As pointed out by Martínez-Lope *et al.* this implies that the strain is not only due to tilting of VO$_6$ octahedra. An additional contribution proposed below for LaMnO$_3$ is from local strain heterogeneities associated with the Jahn–Teller distortion of individual octahedra which act to suppress coupling of the order parameter for octahedral tilting with the macroscopic strain.

2.4. Order-parameter coupling

Coupling between octahedral tilting and Jahn–Teller order parameters in the $P2_1/a$ structure is described by (from §3 of Carpenter & Howard, 2009)

$$\lambda_{qR3+M3+} a_{JT}^2 q_2^2 + 2\lambda_{qR3+R4+} a_{JT}^2 q_4^2 + \frac{3}{2}\lambda'_{qR3+R4+} a_{JT}^2 q_4^2. \quad (15)$$

All the terms are biquadratic, *i.e.* of the form $\lambda q_{JT}^2 q_{tilt}^2$. The most overt evidence of this coupling could appear in the renormalization of the critical temperature, T_c, effectively as

$$T_{c,JT}^* = T_{c,JT} - \frac{\lambda q_{tilt}^2}{a}. \quad (16)$$

A second-order transition at $T_{c,JT}$ in a crystal with no tilting would become $T_{c,JT}^*$ in a crystal with some fixed degree of tilting. Comparison of the data for *Pnma* (no JT) $\rightarrow P2_1/a$ transition temperatures of Miyasaka *et al.* (2003) with data of Martínez-Lope *et al.* (2008) for tilt angles at room temperature shows that a simple trend of increasing or decreasing $T_{c,JT}^*$ with increasing tilt angle is however not observed. Without data for the separate tilt angles relating to q_2 and q_4, it is not possible to further test this prediction of the full influence of coupling. On
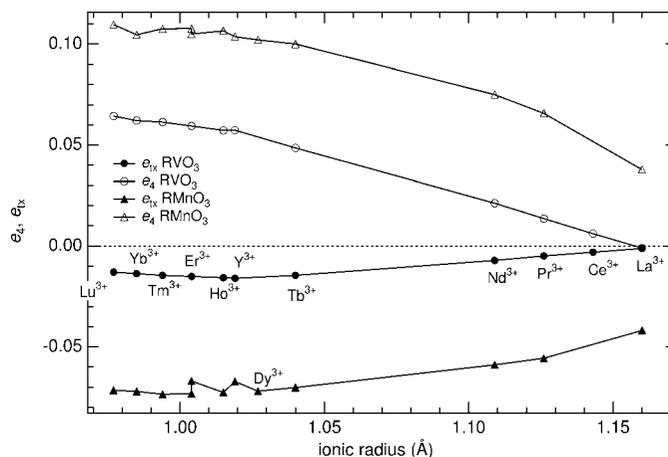
Figure 4
Variation of symmetry-adapted strains as a function of the ionic radius of the R cation at room temperature for RVO$_3$ and RMnO$_3$ perovskites, as calculated from the lattice-parameter data of Alonso *et al.* (2000), Tachibana *et al.* (2007) and Martínez-Lope *et al.* (2008). Ionic radii are those from Table 1 of Martínez-Lope *et al.* (2008; after Shannon, 1976). In vanadates, the strains are due to octahedral tilting transitions from a parent cubic (*Pm$\bar{3}$m*) structure to the *Pnma* structure. In manganites the strain is due to both octahedral tilting and to the cooperative Jahn–Teller transition. For both systems the magnitude of the strains reduces with increasing ionic radius of the A-site cation.

Figure 3
Variation of e_5^2 with Δe_{tx} for CeVO$_3$, where Δe_{tx} is the change in tetragonal strain due to the *Pnma* $\rightarrow P2_1/a$ transition (see Fig. 2). The linear correlation at temperatures above T_N (straight line fit to the data) is consistent with $e_5^2 \propto \Delta e_{tx} \propto a_{JT}^2$.

the other hand, if the critical temperatures for Jahn–Teller ordering and octahedral tilting are widely separated, it should be expected that the influence of one order parameter on the other would be small, such that the tilt angle across a Jahn-–Teller transition would not show much of a deflection. This is indeed consistent with the behaviour observed.

On the basis of a microscopic model, Mizokawa *et al.* (1999) argued that M_2^+ ordering is stabilized relative to R_3^+ ordering due to the influence of octahedral tilting. In the present context, this would be equivalent to asserting that the coupling terms favour the *Pnma* Jahn–Teller structure ahead of the $P2_1/a$ structure. However, as seen from the discussion of octahedral tilting in §2.1, the strain which should be most sensitive to the R_4^+ tilt actually decreases at the $P2_1/a \rightarrow Pnma$ transition. In detail the direct order-parameter coupling terms permitted by symmetry show that the coupling of Jahn–Teller order parameters with the different tilt order parameters is quite subtle. For the *Pnma* Jahn–Teller structure, the direct coupling terms would be

$$(\lambda_{qM2+M3+} + \lambda'_{qM2+M3+})q_{2JT}^2 q_2^2 + 2\lambda_{qM2+R4+}q_{2JT}^2 q_4^2$$
$$+ \lambda_{qM2+M3+R4+}q_{2JT}q_2 q_4^2. \tag{17}$$

The key point is that a complete analysis of how the tilting influences stability would require separation of q_2 and q_4 tilts rather than the use of a single effective tilt angle which includes both components.

The magnitudes of both e_4 and e_{tx} are lower in the *Pnma* structure than they are in the $P2_1/a$ structure, indicating that there are subtle changes in the values of the coupling coefficients and/or the evolution of the order parameters for the two structure types. There is also a difference in the volume strain, revealed by the data of Marquina *et al.* (2005) for YVO$_3$. The variation of unit-cell volume with temperature derived from the linear thermal expansion data is given in Fig. 1. A standard baseline function, $V_o = y_0 + y_1\Theta_{so}\coth(\Theta_{so}/T)$ (Meyer *et al.*, 2000, 2001; Sondergeld *et al.*, 2000; Carpenter *et al.*, 2003; after Salje *et al.*, 1991) has been fit to data in the interval 200–300 K. This gives a saturation temperature of $\Theta_{so} = 128 \pm 48$ K, which is not atypical for perovskites (*e.g.* Hayward *et al.*, 2002), and a curve which extrapolates through data for the $P2_1/a$ structure. Any change in volume strain associated with the *Pnma* (no JT) $\rightarrow P2_1/a$ transition is essentially zero, consistent with the finding of Bizen *et al.* (2007) that the transition temperature is independent of pressure. There is then a change of volume strain of ~ -0.0015 at the $P2_1/a \rightarrow Pnma$ (JT) transition, consistent with the increase in transition temperature with increasing pressure shown by Bizen *et al.* (2007). Sage *et al.* (2007) described essentially the same volume evolution for GdVO$_3$, and Zhou *et al.* (2007) have reported a similar effect of pressure on the $P2_1/a \rightarrow Pnma$ transition in LuVO$_3$. Thus, the *Pnma* Jahn–Teller structure has a smaller total shear strain and a slightly different volume relaxation than the $P2_1/a$ structure. These differences are uncalibrated in terms of the energy changes which they might represent, however.

The Néel temperature is discernable in the strain variations of CeVO$_3$, but not in strains for the other systems analysed here. If there is coupling between the magnetic order parameter and the Jahn–Teller/tilt order parameters *via* a common strain, it is presumably greatest for the large R cations, where there is also the smallest difference between the Néel temperature and Jahn–Teller transition temperature.

In summary, Jahn–Teller and octahedral tilting transitions in RVO$_3$ structures are both accompanied by significant strain/order-parameter coupling which allows the evolution of the separate order-parameter components to be investigated. There are subtle differences in the strain behaviour of the two types of Jahn–Teller structures, but the significance of these in relation to their possible contribution to relative stability has not been calibrated. Other structure types have been reported, including a possible triclinic structure in YVO$_3$ at low temperatures (Ulrich *et al.*, 2003; Tsvetkov *et al.*, 2004), implying that there could be more complex pathways through the possible transition hierarchies shown in Figs. 3 and 4 of Carpenter & Howard (2009).

2.5. Thermodynamic character of the transitions

The *Pnma* (no JT) $\rightarrow P2_1/a$ transition is known to be continuous and, in that sense, second order in character (Blake *et al.*, 2001, 2002; Ren *et al.*, 2003; Tsvetkov *et al.*, 2004). The curvature shown by the strain data show, further, that for at least some vanadates there are contributions to the free energy from a sixth-order term in the order parameter (246 Landau potential). The form of the excess heat-capacity curve associated with the *Pnma* (no JT) $\rightarrow P2_1/a$ transition in YVO$_3$ (Fig. 5 of Blake *et al.*, 2002) is consistent with this in showing a tendency towards having a λ shape. In their analysis of the heat-capacity results, Blake *et al.* (2002) also pointed out that the entropy change is much lower than the configurational entropy expected for pure order/disorder behaviour. The $Pnma \rightarrow P2_1/a$ transition appears to display characteristics which are closer to the displacive limit than to the order/disorder limit.

3. Jahn-Teller + octahedral tilting transitions in (La,Ba)MnO₃ perovskites

3.1. Strain analysis of LaMnO₃

The *Pnma* (JT + tilt) structure of LaMnO$_3$ develops by $M_3^+ + R_4^+$ tilting before undergoing Jahn–Teller ordering according to M_2^+: $R\bar{3}c \leftrightarrow Pnma$ (tilted) $\leftrightarrow Pnma$ (tilted + JT). The two phase transitions occur at ~ 1010 and 750 K (Norby *et al.*, 1995; Rodríguez-Carvajal *et al.*, 1998; Mandal *et al.*, 2001; Mandal & Ghosh, 2003; Sánchez *et al.*, 2003; Chatterji *et al.*, 2003, 2004, 2006; Qiu *et al.*, 2005).

A formal strain analysis is again revealing of order-parameter evolution through the phase transitions. Individual lattice parameters for LaMnO$_3$ have been reproduced in Fig. 5(a) from Fig. 3 of Chatterji *et al.* (2003), and used to determine values for the shear strains e_4 and e_{tx}. The same approximation as applied in the case of vanadates was used to

estimate a_o. Unit-cell volume data, for the small pseudocubic cell, are reproduced in Fig. 5(b). These have been used to determine values for the volume strain, V_s, associated with the Jahn–Teller transition according to the usual definition

$$V_s = \frac{V - V_o}{V_o}. \qquad (18)$$

In this case, values for the reference parameter, V_o, were obtained by fitting a straight line to data for the unit-cell volume above 750 K and extrapolating to lower temperatures. The resulting strains are shown in Fig. 5(c) and display the characteristic pattern of a classical coelastic, first-order structural phase transition at ~ 750 K.

Structural data of Rodríguez-Carvajal et al. (1998) and Chatterji et al. (2003) are consistent with the view that the Pnma phase of LaMnO₃ has $q_2 \neq 0$, $q_4 = q_6 \neq 0$ and $q_{2JT} = 0$ at

$T > \sim 750$ K. The strains are close to zero in spite of the total octahedral tilt angle about [111] being more than 10° (Rodríguez-Carvajal et al., 1998), which implies that the coupling coefficients λ_1–λ_5 in (6)–(10) are small. Below ~ 750 K $q_{2JT} \neq 0$ but the tilt angle increases only slightly (Fig. 5c), consistent with q_2 and q_4 remaining almost constant. Large strains (up to $\sim 4\%$) immediately develop and, if q_2, q_4 hardly vary and λ_1–λ_5 are small, this requires that the coupling coefficients λ_{tM2+}, $\lambda_{eM2+M3+}$ and λ_{aM2+} are large. An internal inconsistency is immediately apparent, however, in that e_{tx} and e_4 should then show quite different variations with temperature since the former depends on q_{2JT}^2 [see (6)] and the latter on q_{2JT} [see (8)]. In reality, all three of the strains arising at the ~ 750 K transition vary almost linearly with each other (Fig. 6), which can only occur if they are each due almost exclusively to coupling with the square of the octahedral tilt components. This requires that λ_{tM2+}, $\lambda_{eM2+M3+}$ and λ_{aM2+} are small. A straightforward solution of the apparent inconsistency is that λ_1–λ_5 are themselves dependent on q_{2JT}. The lowest order dependence allowed by symmetry has $\lambda_i = \lambda_i' q_{JT}^2$, giving strain/tilt coupling relationships of the form $e \propto \lambda_i' q_{JT}^2 q_{tilt}^2$. In this case the strains would be zero in the Pnma phase at $T > \sim 750$ K and would all scale with q_{2JT}^2 if the tilt angles do not vary much through the transition point. The fit to e_4 in Fig. 5(c) is a first-order solution to a standard Landau 246 potential with negative fourth-order coefficient, showing, further, that the evolution of q_{2JT}^2 can be described in terms of a simple mean-field pattern.
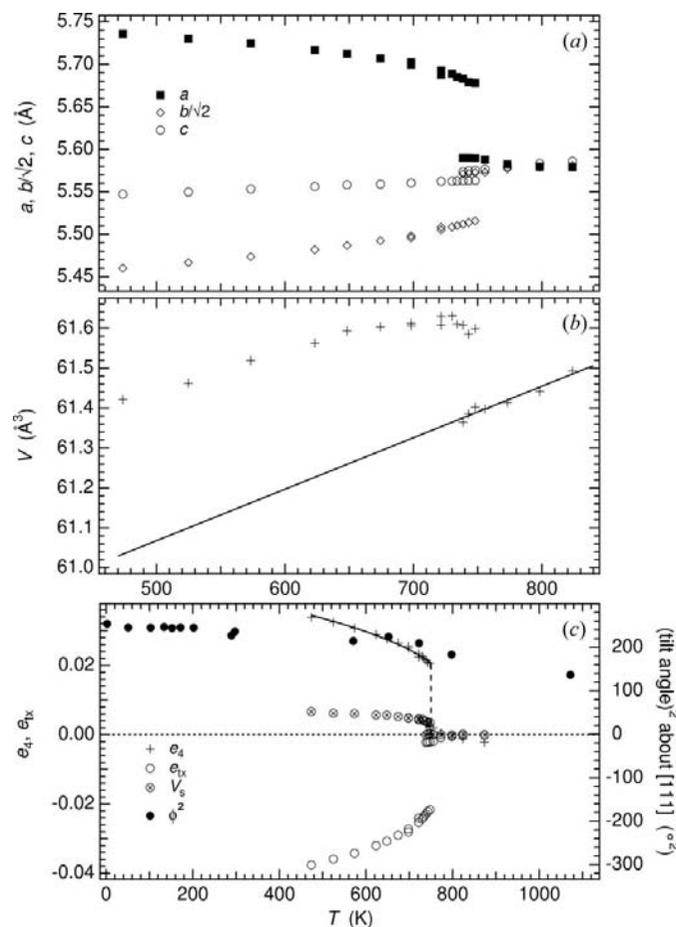
Figure 5
Lattice-parameter data for LaMnO₃, reproduced from Chatterji et al. (2003), and symmetry-adapted strains derived from them. Unit-cell volume is given for the small pseudocubic cell. Volume strain, V_s, was determined with respect to the reference volume, V_o, given by the straight-line fit to the data at $T > 750$ K. The symmetry-adapted strains in (c) follow the classical pattern of a first-order phase transition driven by a single order parameter. The solid curve is a fit to e_4 using the solution for a Landau 246 potential with a negative fourth-order coefficient and the transition temperature set at 750 K ($T_c = 646$ K, step at 750 K = 0.02064). There is very little change in octahedral tilt angles through the transition according to data reproduced from Rodríguez-Carvajal et al. (1998, filled circles, right axis).
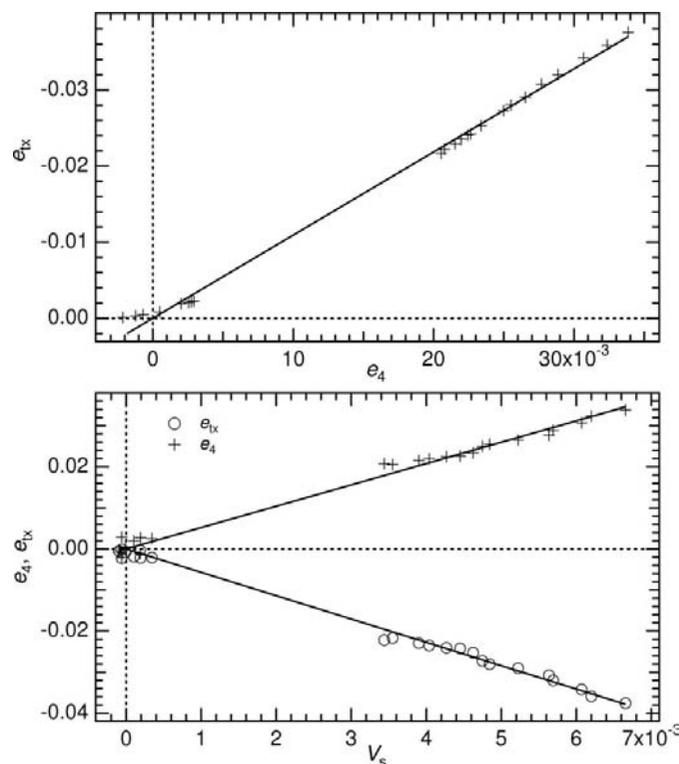
Figure 6
Strain–strain relationships for LaMnO₃. Each of the symmetry-adapted strains arising at the Pnma (tilted) ↔ Pnma (tilted + JT) transition varies almost linearly with each of the other strains.

Additional evidence that the Jahn-Teller transition in $LaMnO_3$ is manifest through the dependence of the strain/tilt coupling coefficients on q_{2JT}^2 is provided by the variations of shear strains with pressure. Owing to the positive volume strain associated with the Jahn–Teller ordering transition, the effect of increasing pressure is expected to be stabilization of structures with octahedral tilting only, as confirmed by Loa *et al.* (2001). Lattice-parameter data from Fig. 2 of Loa *et al.* (2001) have been used here to calculate macroscopic shear strains [with the usual approximation $a_o = (a_c b_c c_c)^{1/3}$], and these are shown in Fig. 7. A clear break in slope occurs in e_4 at ~ 16 GPa, which corresponds closely to the pressure at which, according to Loa *et al.* (2001), the MnO_6 octahedra, on average, finally lose their individual JT distortions. At $P > 16$ GPa, e_4 is expected to scale with q_4^2 [see (8)] and the linear decrease with increasing pressure is consistent with a reduction in the tilt angle towards a second-order transition at some much higher pressure to a structure without tilting. If the tilt angles do not vary greatly at the Jahn–Teller transition pressure of ~ 16 GPa and $\lambda_{eM2+M3+}$ is small, as when temperature is the applied variable, the change in e_4 shown as Δe_4 in Fig. 7 is due to the Jahn–Teller transition alone. A linear dependence of Δe_4 can be described using $\lambda_5 = \lambda_5' q_{JT}^2 + \lambda_5''$ (where λ_5'' is constant) and $q_{JT}^2 \propto (P_c - P)$. In other words, the Jahn–Teller transition displays classical (mean-field) second-order character with $P_c \simeq 16$ GPa. The evolution of e_{tx} is inevitably more complex because of the dependence on both q_2 and q_4 [see (6)].

It is known from a recent study of the octahedral tilting transition in $La_{0.6}Sr_{0.1}TiO_3$, which has 30% of the *A* sites vacant, that cation disordering between crystallographic sites suppresses coupling of the tilt order parameter with macroscopic strain, but barely influences the octahedral tilt angles or the transition temperature (Howard *et al.*, 2007). The mechanism for this almost certainly involves the development of local distortions or strain heterogeneities when differently sized cations occupy adjacent crystallographic sites in a disordered manner, and a similar mechanism can be envisaged for $LaMnO_3$. Sánchez *et al.* (2003), Qiu *et al.* (2005) and Bozin *et al.* (2006) seem to have shown definitively that individual MnO_6 octahedra in $LaMnO_3$ retain a degree of Jahn–Teller distortion up to high temperatures. The *Pnma* (tilted) $\leftrightarrow$ *Pnma* (tilted + JT) transition at ~ 750 K is effectively then due to a change from ordered to disordered arrangements of the octahedra, with any ordering of the orientations above 750 K occurring only within clusters up to ~ 16 Å in diameter (Sánchez *et al.* 2003; Qiu *et al.* 2005). Sánchez *et al.* (2003) also highlighted the importance of strain in mediating the ordering process. Disordering of distorted octahedra must be accompanied by the development of local strains in the same manner as has been argued for the disordering of cations and vacancies in $La_{0.6}Sr_{0.1}TiO_3$. Structural heterogeneity in the form of local strain gradients hinders the development of long-range correlations of microscopic strains which would normally make up the macroscopic strain that accompanies octahedral tilting. The outcome at a macroscopic scale is that the strain/tilt coupling parameters have a strong dependence on the second order parameter. Indirect evidence of such local strain behaviour on a unit-cell scale in silicate and oxide solid solutions is provided by line broadening in powder IR absorption spectra (Boffa Ballaran *et al.*, 1998; Atkinson *et al.*, 1999; Carpenter *et al.*, 1999; Salje *et al.*, 2000; Meyer *et al.*, 2002; Carpenter & Boffa Ballaran, 2001; Carpenter, 2002; Tarantino *et al.*, 2002).

3.2. Chemical doping

A different perspective on the importance of local heterogeneous strains in manganite perovskites is provided by the evolution of macroscopic strains in the $La_{1-x}Ba_xMnO_3$ solid solution. Lattice-parameter data of Chatterji *et al.* (2004) for $x = 0.025$–0.1 have been used to determine symmetry-adapted strains through the *Pnma* $\leftrightarrow$ *Pnma* transition at several different compositions, and these are presented in Fig. 8. Volume strains calculated in the same way as for $LaMnO_3$ show a decrease in the marked discontinuity at the transition point and a trend towards linear behaviour when Ba is added (Fig. 8*a*). The pattern of evolution of both e_{tx} and e_4 is qualitatively the same, although there is a small deviation from cubic lattice geometry in the doped samples above their respective transition temperatures. As in pure $LaMnO_3$, the shear strains, e_{tx} and e_4, are linearly related (Fig. 8*c*), and the same arguments apply in relation to their origin. The evolution of V_s, e_{tx} and e_4 is therefore expected to reveal the evolution with temperature and composition of q_{2JT}^2. On this basis V_s for the *Pnma* (tilted) $\leftrightarrow$ *Pnma* (tilted + JT) transition shows the temperature dependence of a classical first-order transition (Landau 246 potential, negative fourth-order coefficient) at $x = 0, 0.025$, close to tricritical character [Landau 26 potential, $q^4 \propto (T_c - T)$] at $x = 0.05$, 246 character with positive fourth-order coefficients at $x = 0.075$ and second-order character [Landau 24 potential, $q^2 \propto (T_c - T)$] at $x = 0.1$ (Fig. 8*a*). The magnitudes of the strains all diminish with increasing Ba

Figure 7
Symmetry-adapted strain variations with pressure for $LaMnO_3$, as determined from lattice-parameter data given in Fig. 2 of Loa *et al.* (2001) and the approximation $a_o = (a_c b_c c_c)^{1/3}$. Straight lines have been fit to data at $P \geq 16$ GPa and $P \leq 16$ GPa. The difference between these, Δe_4, is interpreted in terms of a second-order transition $[\Delta e_4 \propto q_{JT}^2 \propto (P_c - P), P_c \simeq 16$ GPa] driven by cooperative Jahn–Teller distortions.

content, consistent with suppression of the strain/tilt coupling by local strain heterogeneities owing to substitution of Ba^{2+} for La^{3+} and replacement of some $Mn^{3+}O_6$ octahedra by $Mn^{4+}O_6$ octahedra. A reduction in the strength of coupling will be at least a contributory factor in the change from first-order character to second-order character for the transition through renormalization of the fourth-order Landau coefficient in the usual manner (see also, Maitra *et al.*, 2004).
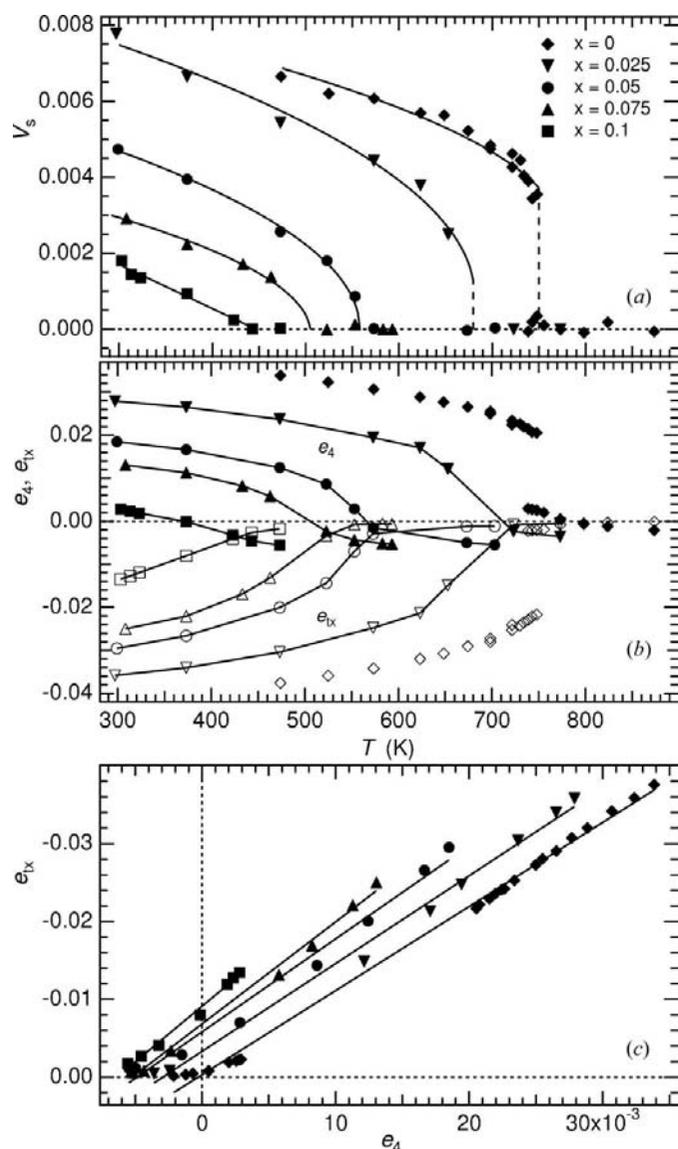
Figure 8
Symmetry-adapted strains calculated from the lattice-parameter data of Chatterji *et al.* (2004) for $La_{1-x}Ba_xMnO_3$ with $x = 0.025$, 0.05, 0.075 and 0.1. Strains for $x = 0$ are those given in Fig. 5(c). (a) The volume strains have been fit with standard solutions to a Landau expansion assuming that V_s scales with the square of a single order parameter. On this basis the transition is first order in character at $x = 0$, 0.025, tricritical at $x = 0.05$ and second order at $x = 0.1$. (b) The *Pnma* (tilted) ↔ *Pnma* (tilted + JT) transition in doped samples is marked by crossing of the trends for e_{tx} and e_4 and the appearance of a volume strain. (c) Symmetry-adapted shear strains vary linearly with each other at each composition, although they each have a different origin.

Substitution of Ca or Sr for La in $La_{1-x}Sr_xMnO_3$ and $La_{1-x}Ca_xMnO_3$ causes essentially the same change in lattice parameters through the *Pnma* (tilted) ↔ *Pnma* (tilted + JT) transition as is seen when Ba is substituted in $La_{1-x}Ba_xMnO_3$ (Chatterji *et al.*, 2002, 2004, 2006). The transition changes from first order to second order in character and the magnitude of the total strains reduces with increasing dopant level in each case. Tilt angles also vary very little through the transition in Sr-doped samples (Chatterji *et al.*, 2002). A classical Landau free-energy expansion includes truncation for the entropy after the term in q^2 and provides effective descriptions of the order-parameter evolution for phase transitions which are closer to the displacive limit than to the order/disorder limit. The tendency towards Landau second-order character for the Jahn–Teller transition is therefore consistent with displacive behaviour overall, at least in doped samples, notwithstanding the evidence for disordering of distorted MnO_6 octahedra in pure $LaMnO_3$. In this context, Sánchez *et al.* (2003) also found that the entropy change associated with the Jahn–Teller transition in $LaMnO_3$ is somewhat less than expected for a pure order/disorder process.

A monoclinic phase has been reported in the $La_{1-x}Ba_xMnO_3$ system by Rotiroti *et al.* (2005). Their assignments to space group $I2/c$ and unit cell $\sqrt{2}a_p \times \sqrt{2}a_p \times 2a_p$, $\beta \neq 90°$, for a sample with composition $La_{0.815}Ba_{0.185}MnO_3$, is a different setting for structures with $C2/c$ symmetry and lattice vectors $(2,\bar{1},\bar{1})(0,1,\bar{1})(0,1,1)$ listed in Table 1 of Carpenter & Howard (2009). Either of the Γ_3^+ and R_3^+ Jahn–Teller ordering schemes could be accommodated within this structure, but the refined atomic coordinates showed no overt evidence for JT distortions of the octahedra. Owing to the existence of third-order invariants, the $R\bar{3}c \leftrightarrow C2/c$ transition must be first order in character. Radaelli *et al.* (1996) also found a first order, octahedral tilting phase transition at a nearby composition, $La_{0.7}Ba_{0.3}MnO_3$, but with a symmetry change $R\bar{3}c \leftrightarrow Imma$ and a transition temperature of ~ 175 K.

Burgy *et al.* (2001) described doped transition metal oxides as being intrinsically inhomogeneous, and the heterogeneity of two phase intergrowths on nanometer or micrometer length scales appears to be integral to the development of colossal magnetoresistance properties in manganite solid solutions (Moreo *et al.*, 1999; Uehara *et al.*, 1999; Uehara & Cheong, 2000; Fäth *et al.*, 1999; Dagotto *et al.*, 2001; Renner *et al.*, 2002; Zhang *et al.*, 2002; Mathur & Littlewood, 2003; Salamon & Jaime, 2001; Ahn *et al.*, 2004; Goodenough, 2004; Israel *et al.*, 2007). Goodenough (2004) has also referred to spinodal decomposition of orthorhombic manganites into separate phases with and without JT order. A specific decomposition mechanism can occur in solid solutions due to phase transitions which are second order in character, as has been recognized in silicate minerals for example (Carpenter, 1980, 1981, 1994). Cation ordering drives precipitation in these materials and, if the transition is second order, a conditional spinodal results in characteristic coherent precipitation microstructures on an electron optical scale. By analogy, a two-phase field of JT ordered and disordered phases could

occur along the extension of the second-order *Pnma* ↔ *Pnma* transition in La(Ba,Ca,Sr) manganite solid solutions at low temperatures, though with different compositions.

3.3. Isosymmetric behaviour

Isosymmetric phase transitions are expected to be first order in character essentially because a term linear in the driving order parameter is allowed in the excess free energy (Christy, 1995). There are a number of examples of isosymmetric transitions which are indeed discrete and first order in character, including, for example, in ice VIII (Klug *et al.*, 2004), α-PbF$_2$ (Haines *et al.*, 1998) and silicate minerals such as pyroxenes (Hugh-Jones & Angel, 1994; Ohi *et al.*, 2008). The magnitude of the discontinuity in thermodynamic properties can be small, however, as in the case of NH$_4$PF$_6$ (Swainson *et al.*, 2002). In principle, LaMnO$_3$ should not be an exception since there is a term linear in q_{2JT} among the coupling terms for the *Pnma* Jahn–Teller structure [see (17)]. The strain behaviour shows, however, that renormalization of the tilt/strain coupling coefficient could be an important, if not dominant, process in driving the transition and this would allow nearly second-order character if the coupling coefficient $\lambda_{qM2+M3+R4+}$ is small/negligible. The strains shown in Figs. 7 and 8 do not have sufficient resolution to confirm that there is no discontinuity at the transition point in LaMnO$_3$ at high pressures or in Ba-doped samples, but the evolution away from the transition point, at least, is consistent with second-order character.

3.4. Correlations between strain and electrical resistivity

The Jahn–Teller transition in LaMnO$_3$ is accompanied by a large change in electrical resistivity, ρ (Zhou & Goodenough, 1999; Mandal *et al.*, 2001; Mandal & Ghosh, 2003). Chatterji *et al.* (2004, 2006) found that variations in ρ as a function of temperature and Ca/Ba doping closely mirror the patterns of volume change. The first-order transition in LaMnO$_3$ is associated with large and discontinuous steps in both properties. Again in parallel with data for unit-cell volume, increasing dopant levels not only cause the change in ρ to become continuous through the transition, but also substantially reduce differences between the values for tilted-only structures and tilted + JT ordered structures. Here it has been shown that the same correlation occurs for the shear strains, and it has been argued that the macroscopic strain behaviour could be strongly influenced by local strain effects. At high pressures the tilted form of LaMnO$_3$ without Jahn–Teller order ($P > \sim 18$ GPa) retains significant distortions from cubic lattice geometry. If local strain behaviour is a factor in suppressing the coupling of octahedral tilting with macroscopic strains, the high-pressure phase is presumably more homogenous on a length scale of up to a few unit cells than the equivalent high-temperature phase. The high-pressure phase also does not have the reduced resistivity of the high-temperature phase (Loa *et al.*, 2001). Pseudocubic lattice geometry thus seems to be required for metallic conductivity,

suggesting that strain heterogeneity could be a determinative factor for both.

3.5. *R*MnO$_3$ systematics

As with vanadates, systematic variations in lattice geometry with ionic radius for ABX_3 perovskites at room temperature can also be examined from the perspective of macroscopic strain. Values of e_4 and e_{tx} determined using the lattice-parameter data of Alonso *et al.* (2000) and Tachibana *et al.* (2007) for *R*MnO$_3$ have been added to Fig. 4 for comparison. At up to $\sim 10\%$ these strains are larger than occur in more typical ferroelastic materials, such as Pb$_3$(PO$_4$)$_2$ (Salje *et al.*, 1993; Carpenter *et al.*, 1998). The manganites include JT ordering at room temperature (Alonso *et al.*, 2000; Zhou & Goodenough, 2006; Tachibana *et al.*, 2007), whereas the vanadates do not, but the overall trend is the same – increasing the ionic radius of the *R* cation reduces the macroscopic strain. This pattern of strain variations reflects what appears to be a universal pattern of lattice-parameter variations among *R*TiO$_3$, *R*CrO$_3$, *R*FeO$_3$, *R*NiO$_3$, *R*MnO$_3$, *R*CoO$_3$ and *R*GaO$_3$ perovskites, but the observed trends at large radii are not due simply to tilting of rigid octahedra (Zhou & Goodenough, 2005). The strain evolution with temperature shown by LaMnO$_3$ can be accounted for in terms of the additional effect of local strain heterogeneities causing a suppression of the macroscopic strain coupling with octahedral tilts. If the same mechanism applies in the other perovskite series, it appears that such heterogeneities arise in particular when La is the *A*-site cation. For example, the *Pnma* form of LaVO$_3$ with tilting only has lattice geometry which is very close to being cubic, but orthorhombic strains then develop in the monoclinic phase below the Jahn–Teller transition temperature of ~ 140 K (Ren *et al.*, 2003).

4. Jahn–Teller transitions with Γ_3^+ active

Two examples of Jahn–Teller ordering with Γ_3^+ as the active representation are PrAlO$_3$ (Carpenter *et al.*, 2005) and La$_{0.5}$Ba$_{0.5}$CoO$_3$ (Fauth *et al.*, 2001; Nakajima *et al.*, 2005). In PrAlO$_3$, the Jahn–Teller ion is on the crystallographic *A* site, but this does not affect the symmetry arguments. The distortions occur below room temperature in a structure which has $R\bar{3}c$ tilting (R_4^+) up to ~ 1860 K (Burbank, 1970; Kjems *et al.*, 1973; Birgeneau *et al.*, 1974; Cohen *et al.*, 1974; Sturge *et al.*, 1975; Lyons *et al.*, 1975; Harley *et al.*, 1973; Fujii *et al.*, 1999; Watanabe *et al.*, 2006). Recent powder neutron diffraction studies suggest that the full transition sequence is $Pm\bar{3}m$ ↔ $R\bar{3}c$ ↔ *Imma* ↔ $C2/m$ (Moussa *et al.*, 2001; Howard *et al.*, 2000; Carpenter *et al.*, 2005). Jahn–Teller distortions are incompatible with trigonal lattice geometry and the $R\bar{3}c$ ↔ *Imma* transition can be understood as occurring because there is a tetragonal strain which is common to both the tilting and electronic order-parameter components

$$e_{tx} = \frac{\left(2\lambda_4 q_4^2 - \lambda_{t\Gamma3+}q_{tx}\right)}{\frac{1}{2}\left(C_{11}^o - C_{12}^o\right)} \tag{19}$$

where

$$q_{tx} = \frac{1}{2}\left(q_{tx} + \sqrt{3}q_{oz}\right) \quad (20)$$

and the *Imma* structure has $q_4 = q_6 \neq 0$, $q_5 = 0$, $q_{oz} = \sqrt{3}q_{tz} \neq 0$. In effect, the $q_4 = q_6$ tilt system acts as an applied field such that a degree of electronic ordering is induced above the Jahn–Teller transition point.

The driving order parameter for the *Imma* $\leftrightarrow$ *C2/m* transition is q_{ox}, where

$$q_{ox} = \frac{1}{2}\left(\sqrt{3}q_{tz} - q_{oz}\right) \quad (21)$$

and this causes the monoclinic distortion through coupling with e_{ox} as

$$e_{ox} = \frac{\left[\sqrt{3}\lambda_4\left(q_4^2 - q_6^2\right) - \lambda_{t\Gamma3+}q_{ox}\right]}{\frac{1}{2}\left(C_{11}^o - C_{12}^o\right)}. \quad (22)$$

Strain analysis of high-resolution powder neutron diffraction data has shown that the *Imma* $\leftrightarrow$ *C2/m* transition is second order in character (Carpenter *et al.*, 2005).

An important difference in the behaviour of Γ_3^+ as the active representation, as opposed to M_2^+ or R_3^+, arises from the fact that there is bilinear coupling between the Jahn–Teller order-parameter components and the symmetry-breaking strains e_{oz} and e_{tz} [the $\lambda_{t\Gamma3+}$ $(q_{oz}e_{oz} - q_{tz}e_{tz})$ term in equation 10 of Carpenter & Howard, 2009]. This causes the Jahn–Teller transitions to be pseudo-proper ferroelastic in character and has additional implications for the possible contributions of local strain heterogeneities. In the case of a second-order transition, the transition temperature, $T_{c,JT}^*$, is given by

$$T_{c,JT}^* = T_{c,JT} + \frac{\lambda_{t\Gamma3+}^2}{a\frac{1}{2}\left(C_{11}^o - C_{12}^o\right)}. \quad (23)$$

Thus, any local strain effects which influence the coupling coefficient $\lambda_{t\Gamma3+}$, comparable to the behaviour observed in $La_{1-x}Ba_xMnO_3$, should cause a renormalization of the transition temperature.

As discussed in Carpenter & Howard (2009), $La_{0.5}Ba_{0.5}CoO_3$ with a disordered distribution of La and Ba on the crystallographic A sites undergoes a $Pm\bar{3}m \leftrightarrow P4/mmm$ transition which has been ascribed to cooperative Jahn–Teller distortions of the CoO_6 octahedra, favoured by at least some of the Co^{3+} and Co^{4+} ions having intermediate spin states (Fauth *et al.*, 2001; Nakajima *et al.*, 2005). First-order character is expected due to the existence of third-order invariants in the free-energy expansion. According to Fauth *et al.* (2001) the structural transition accompanies a ferromagnetic transition at ~ 180 K, while Nakajima *et al.* (2005) placed the structural transition at ~ 140 K, ~ 30–40 K below the magnetic transition. The structural phase transition appears to be a representative example of the Γ_3^+ system, with $q_{tz} \neq 0$, $q_{oz} = 0$, in the absence of octahedral tilting, and the tetragonal strain is expected to evolve according to equation (13) of Carpenter & Howard (2009). Lattice-parameter data obtained by neutron powder diffraction are reproduced in Fig. 9(*a*) from Fig. 3 of Nakajima *et al.* (2005). These have been used to determine e_a

and e_{tz}, using $e_1 = e_2 = (a - a_o)/a_o$ and $e_3 = (c - a_o)/a_o$ where a_o is the reference cubic lattice parameter extrapolated from high temperatures (solid line in Fig. 9*a*). Even bearing in mind the
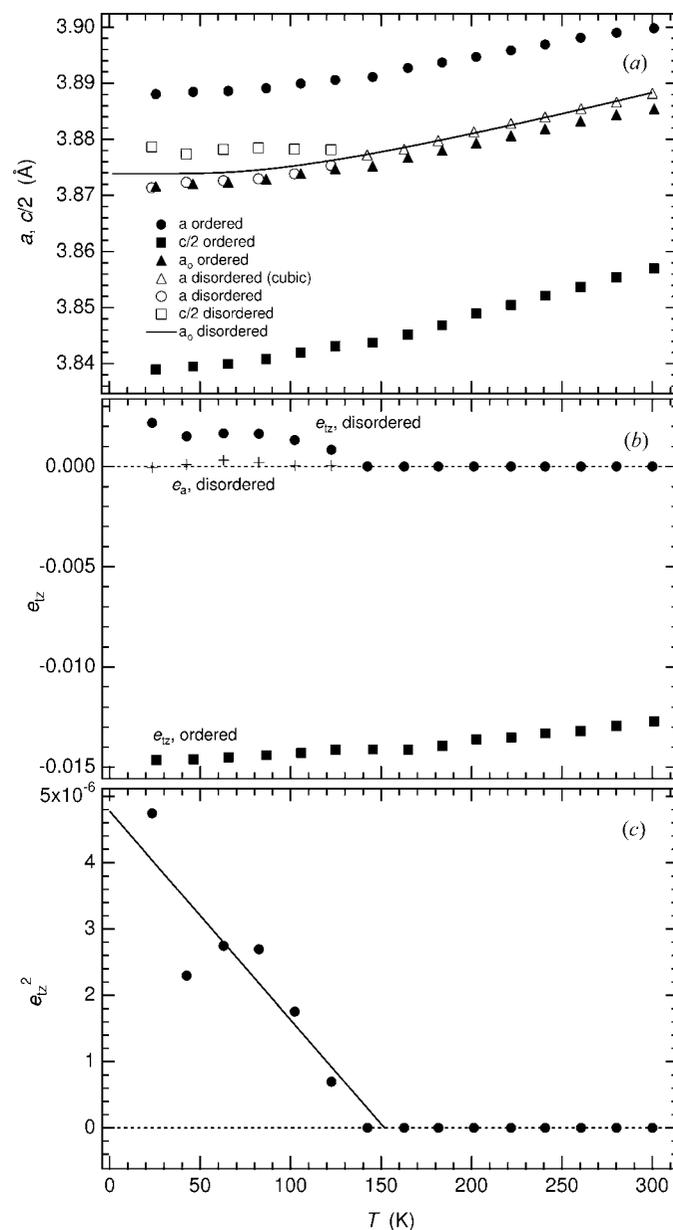
Figure 9
Lattice parameter and spontaneous strain variations associated with a cooperative Jahn–Teller transition in $La_{0.5}Ba_{0.5}CoO_3$ and cation ordering in $LaBaCo_2O_6$. (*a*) Lattice parameters from neutron powder diffraction, reproduced from Fig. 3 of Nakajima *et al.* (2005). The disordered phase has *P4/mmm* and $Pm\bar{3}m$ symmetry below and above ~ 140 K, respectively. The ordered phase has *P4/mmm* symmetry. The reference parameter, a_o, for the disordered phase is shown as a solid curve, which is a fit to the data for the cubic structure using an expression of the form $a_o = A + B\Theta_s\coth(\Theta_s/T)$ (after Salje *et al.*, 1991; Meyer *et al.*, 2000, 2001; Sondergeld *et al.*, 2000; Carpenter *et al.*, 2003); the saturation temperature, Θ_s, was fixed at 150 K. The cubic reference parameter of the ordered phase was calculated as $a_o = (a_c^2 c_c)^{1/3}$. (*b*) Spontaneous strains calculated from the lattice parameters shown in (*a*). (*c*) A straight line, as shown, would imply second-order character for the $Pm\bar{3}m \leftrightarrow P4/mmm$ transition and $T_c = 152$ K ($e_{tz}^2 \propto q_z^2 \propto |T_c - T|$), but the data are scattered and first-order character is also possible.

uncertainty in a_o, the volume strain (e_a) accompanying the transition is essentially zero. Elongation of CoO_6 octahedra along the crystallographic z axis is responsible for the positive value of e_{tz}, but the Jahn–Teller distortion is small and the shear strain reaches a maximum value of only ~ 0.002. Fig. 9(c) shows e_{tz}^2 ($\propto q_{tz}^2$) as a function of temperature. A straight line has been fit to the data as if the transition is second order, with $T_c = 152$ K. In view of the scatter in the data, first-order character cannot be excluded.

Ordering of La and Ba also results in a symmetry reduction from $Pm\bar{3}m$ to $P4/mmm$, although in this case the unit cell of the tetragonal structure is doubled along the crystallographic z axis (Nakajima *et al.*, 2005; Kundu *et al.*, 2007; Rautama *et al.*, 2008). Lattice-parameter data of Nakajima *et al.* (2005), reproduced in Fig. 9(a), have been used to calculate the shear strain, e_{tz}, with the reference parameter determined as $a_o = (a_c^2 c_c)^{1/3}$. (Here a_c and c_c are the dimensions of the tetragonal phase expressed in terms of a primitive pseudo-cubic cell.) Cation ordering causes a large, negative strain (up to ~ -0.015, Fig. 9b). It is inevitable that some coupling between cation ordering and the cooperative Jahn–Teller distortions will occur *via* the common strain, but, because of the opposite sign, such coupling will be unfavourable. This is reflected in the reversal of the shape change of the octahedra, *i.e.* elongation occurs within the (001) plane of the cation ordered structure (Nakajima *et al.*, 2005).

5. Conclusion

From the strain analysis of selected, representative examples of real systems, it appears that the coupled tilting + Jahn–Teller phase transitions in perovskites conform to mean-field behaviour. This is consistent with the underlying role of strain in promoting large interaction lengths. It must be anticipated, therefore, that Landau theory will provide a quantitative description of many of the physical properties (excess heat capacity, susceptibility, elastic constants, hard and soft phonon modes *etc.*), which all depend explicitly on the order parameters. The analysis of $LaMnO_3$ suggests, further, that an important aspect of the strain relaxations is the development of local strain heterogeneity due to mixing and disordering of differently distorted octahedra and to substitution of different cations on the A site of the perovskite structure. Given the link between structural parameters and electronic configuration *via* strain and topology, the overall approach should also provide an additional formal basis for investigating the richness of magnetic and electrical properties of many of these materials.

References

Ahn, K. H., Lookman, T. & Bishop, A. R. (2004). *Nature*, **428**, 401–404.

Alonso, J. A., Martínez-Lope, M. J., Casais, M. T. & Fernández-Díaz, M. T. (2000). *Inorg. Chem.* **39**, 917–923.

Atkinson, A. J., Carpenter, M. A. & Salje, E. K. H. (1999). *Eur. J. Mineral.* **11**, 7–21.

Birgeneau, R. J., Kjems, J. K., Shirane, G. & Van Uitert, L. G. (1974). *Phys. Rev. B*, **10**, 2512–2534.

Bizen, D., Nakatsuka, K., Nakao, H., Murakami, Y., Miyasaka, S. & Tokura, Y. (2007). *J. Magn. Magn. Mater.* **310**, 785–786.

Blake, G. R., Palstra, T. T. M., Ren, Y., Nugroho, A. A. & Menovsky, A. A. (2001). *Phys. Rev. Lett.* **87**, 245501.

Blake, G. R., Palstra, T. T. M., Ren, Y., Nugroho, A. A. & Menovsky, A. A. (2002). *Phys. Rev. B*, **65**, 174112.

Boffa Ballaran, T., Carpenter, M. A., Domeneghetti, M. C., Salje, E. K. H. & Tazzoli, V. (1998). *Am. Mineral.* **83**, 434–443.

Bordet, P., Chaillout, C., Marezio, M., Huang, Q., Santoro, A., Cheong, S.-W., Takagi, H., Oglesby, C. S. & Batlogg, B. (1993). *J. Solid State Chem.* **106**, 253–270.

Bozin, E. S., Qiu, X., Schmidt, M., Paglia, G., Mitchell, J. F., Radaelli, P. G., Proffen, Th. & Billinge, S. J. L. (2006). *Physica B*, **385–386**, 110–112.

Burbank, R. D. (1970). *J. Appl. Cryst.* **3**, 112–120.

Burgy, J., Mayr, M., Martin-Mayor, V., Moreo, A. & Dagotto, E. (2001). *Phys. Rev. Lett.* **87**, 277202.

Carpenter, M. A. (1980). *Contrib. Mineral. Petrol.* **71**, 289–300.

Carpenter, M. A. (1981). *Am. Mineral.* **66**, 553–560.

Carpenter, M. A. (1994). *Feldspars and Their Reactions*, edited by I. Parsons, NATO ASI C421, pp. 221–269. Dordrecht: Kluwer Academic Press.

Carpenter, M. A. (2002). *Eur. Mineral. Union Notes Mineral.* **4**, 311–346.

Carpenter, M. A. (2007*a*). *Am. Mineral.* **92**, 309–327.

Carpenter, M. A. (2007*b*). *Am. Mineral.* **92**, 328–343.

Carpenter, M. A., Becerro, A. I. & Seifert, F. (2001). *Am. Mineral.* **86**, 348–363.

Carpenter, M. A. & Boffa Ballaran, T. (2001). *Eur. Mineral. Union Notes Mineral.* **3**, 155–178.

Carpenter, M. A., Boffa Ballaran, T. & Atkinson, A. J. (1999). *Phase Transitions*, **69**, 95–109.

Carpenter, M. A. & Howard, C. J. (2009). *Acta Cryst.* B**65**, 134–146.

Carpenter, M. A., Howard, C. J., Kennedy, B. J. & Knight, K. S. (2005). *Phys. Rev. B*, **72**, 024118.

Carpenter, M. A., Howard, C. J., Knight, K. S. & Zhang, Z. (2006). *J. Phys. Condens. Matter*, **18**, 10725–10749.

Carpenter, M. A., Meyer, H.-W., Sondergeld, P., Marion, S. & Knight, K. S. (2003). *Am. Mineral.* **88**, 534–546.

Carpenter, M. A., Salje, E. K. H. & Graeme-Barber, A. (1998). *Eur. J. Mineral.* **10**, 621–691.

Chatterji, T., Fauth, F., Ouladdiaf, B., Mandal, P. & Ghosh, B. (2003). *Phys. Rev. B*, **68**, 052406.

Chatterji, T., Ouladdiaf, B., Mandal, P., Banyopadhyay, B. & Ghosh, B. (2002). *Phys. Rev. B*, **66**, 054403.

Chatterji, T., Ouladdiaf, B., Mandal, P. & Ghosh, B. (2004). *Solid State Commun.* **131**, 75–80.

Chatterji, T., Riley, D., Fauth, F., Mandal, P. & Ghosh, B. (2006). *Phys. Rev. B*, **73**, 094444.

Christy, A. G. (1995). *Acta Cryst.* B**51**, 753–757.

Cohen, E., Sturge, M. D., Birgeneau, R. J., Blount, E. I. & Van Uitert, L. G. (1974). *Phys. Rev. Lett.* **32**, 232–235.

Dagotto, E., Hotta, T. & Moreo, A. (2001). *Phys. Rep.* **344**, 1–153.

Fäth, M., Freisem, S., Menovsky, A. A., Tomioka, Y., Aarts, J. & Mydosh, J. A. (1999). *Science*, **285**, 1540–1542.

Fauth, F., Suard, E. & Caignaert, V. (2001). *Phys. Rev. B*, **65**, 060401.

Fujii, H., Hidaka, M. & Wanklyn, B. M. (1999). *Phase Transitions*, **70**, 115–132.

Goodenough, J. B. (2004). *Rep. Prog. Phys.* **67**, 1915–1993.

Goto, T., Kimura, T., Laws, G., Ramirez, A. P. & Tokura, Y. (2004). *Phys. Rev. Lett.* **92**, 257201.

Haines, J., Léger, J. M. & Schulte, O. (1998). *Phys. Rev. B*, **57**, 7551–7555.

Harley, R. T., Hayes, W., Perry, A. M. & Smith, S. R. P. (1973). *J. Phys. C*, **6**, 2382–2400.

Hayward, S. A., Redfern, S. A. T. & Salje, E. K. H. (2002). *J. Phys. Condens. Matter*, **14**, 10131–10144.

Howard, C. J., Kennedy, B. J. & Chakoumakos, B. C. (2000). *J. Phys. Condens. Matter*, **12**, 349–365.

Howard, C. J., Zhang, Z., Carpenter, M. A. & Knight, K. S. (2007). *Phys. Rev. B*, **76**, 054108.

Hugh-Jones, D. & Angel, R. J. (1994). *Am. Mineral.* **79**, 405–410.

Israel, C., Calderón, M. J. & Mathur, N. D. (2007). *Nat. Mater.* **10**, 24–32.

Kimura, T., Goto, T., Shintani, H., Ishizaka, K., Arima, T. & Tokura, Y. (2003). *Nature*, **426**, 55–58.

Kjems, J. K., Shirane, G., Birgeneau, R. J. & Van Uitert, L. G. (1973). *Phys. Rev. Lett.* **31**, 1300–1303.

Klug, D. D., Tse, J. S., Liu, Z., Gonze, X. & Hemley, R. J. (2004). *Phys. Rev. B*, **70**, 144113.

Kundu, A. K., Rautama, E.-L., Boullay, Ph., Caignaert, V., Pralong, V. & Raveau, B. (2007). *Phys. Rev. B*, **76**, 184432.

Loa, I., Adler, P., Grzechnik, A., Syassen, K., Schwarz, U., Hanfland, M., Rozenberg, G. Kh., Gorodetsky, P. & Pasternak, M. P. (2001). *Phys. Rev. Lett.* **87**, 125501.

Lufaso, M. W. & Woodward, P. M. (2004). *Acta Cryst.* B**60**, 10–20.

Lyons, K. B., Birgeneau, R. J., Blount, E. I. & Van Uitert, L. G. (1975). *Phys. Rev. B*, **11**, 891–900.

Maitra, T., Thalmeier, P. & Chatterji, T. (2004). *Phys. Rev. B*, **69**, 132417.

Mandal, P., Bandyopadhyay, B. & Ghosh, B. (2001). *Phys. Rev. B*, **64**, 180405.

Mandal, P. & Ghosh, B. (2003). *Phys. Rev. B*, **68**, 014422.

Marquina, C., Sikora, M., Ibarra, M. R., Nugroho, A. A. & Palstra, T. T. M. (2005). *J. Magn. Magn. Mater.* **290–291**, 428–430.

Martínez-Lope, M. J., Alonso, J. A., Retuerto, M. & Fernández-Díaz, M. T. (2008). *Inorg. Chem.* **47**, 2634–2640.

Mathur, N. & Littlewood, P. (2003). *Phys. Today*, **56**, 25–30.

McKnight, R. E. A., Howard, C. J. & Carpenter, M. A. (2009). *J. Phys. Condens. Matter*, **21**, 015901.

Meyer, H.-W., Carpenter, M. A., Becerro, A. I. & Seifert, F. (2002). *Am. Mineral.* **87**, 1291–1296.

Meyer, H.-W., Carpenter, M. A., Graeme-Barber, A., Sondergeld, P. & Schranz, W. (2000). *Eur. J. Mineral.* **12**, 1139–1150.

Meyer, H.-W., Marion, S., Sondergeld, P., Carpenter, M. A., Knight, K. S., Redfern, S. A. T. & Dove, M. T. (2001). *Am. Mineral.* **86**, 566–577.

Miyasaka, S., Okimoto, Y., Iwama, M. & Tokura, Y. (2003). *Phys. Rev. B*, **68**, 100406.

Mizokawa, T., Khomskii, D. I. & Sawatzky, G. A. (1999). *Phys. Rev. B*, **60**, 7309–7313.

Moreo, A., Yunoki, S. & Dagotto, E. (1999). *Science*, **283**, 2034–2040.

Moussa, S. M., Kennedy, B. J., Hunter, B. A., Howard, C. J. & Vogt, T. (2001). *J. Phys. Condens. Matter*, **13**, L203–L209.

Muñoz, A., Alonso, J. A., Casais, M. T., Martínez-Lope, M. J., Martínez, J. L. & Fernández-Díaz, M. T. (2003*a*). *J. Mater. Chem.* **13**, 1234–1240.

Muñoz, A., Alonso, J. A., Casáis, M. T., Martínez-Lope, M. J., Martínez, J. L. & Fernández-Díaz, M. T. (2003*b*). *Phys. Rev. B*, **68**, 144429.

Muñoz, A., Alonso, J. A., Casais, M. T., Martínez-Lope, M. J., Martínez, J. L. & Fernández-Díaz, M. T. (2004*a*). *Chem. Mater.* **16**, 1544–1550.

Muñoz, A., Alonso, J. A., Casais, M. T., Martínez-Lope, M. J., Martínez, J. L. & Fernández-Díaz, M. T. (2004*b*). *J. Magn. Magn. Mater. B*, **272–276**, 2163–2164.

Nakajima, T., Ichihara, M. & Ueda, Y. (2005). *J. Phys. Soc. Jpn*, **74**, 1572–1577.

Norby, P., Krogh Andersen, I. G., Krogh Andersen, E. & Andersen, N. H. (1995). *J. Solid State Chem.* **119**, 191–196.

Ohi, S., Miyake, A, Shimobayashi, N., Yashima, M. & Kitamura, M. (2008). *Am. Mineral.* **93**, 1682–1685.

Okazaki, A. (1969*a*). *J. Phys. Soc. Jpn*, **26**, 870.

Okazaki, A. (1969*b*). *J. Phys. Soc. Jpn*, **27**, 518.

Qiu, X., Proffen, Th., Mitchell, J. F. & Billinge, S. J. L. (2005). *Phys. Rev. Lett.* **94**, 177203.

Radaelli, P. G., Marezio, M., Hwang, H. Y. & Cheong, S.-W. (1996). *J. Solid State Chem.* **122**, 444–447.

Rautama, E.-L., Boullay, P., Kundu, A. S., Caignaert, V., Pralong, V., Karppinen, M. & Raveau, B. (2008). *Chem. Mater.* **20**, 2742–2750.

Reehuis, M., Ulrich, C., Pattison, P., Ouladdiaf, B., Rheinstädter, M. C., Ohl, M., Regnault, L. P., Miyasaka, M., Tokura, Y. & Keimer, B. (2006). *Phys. Rev. B*, **73**, 094440.

Ren, Y., Nugroho, A. A., Menovsky, A. A., Strempfer, J., Rütt, U., Iga, F., Takabatake, T. & Kimball, C. W. (2003). *Phys. Rev. B*, **67**, 014107.

Renner, Ch., Aeppli, G., Kim, B.-G., Soh, Y.-A. & Cheong, S.-W. (2002). *Nature*, **416**, 518–521.

Rodríguez-Carvajal, J., Hennion, M., Moussa, F., Moudden, A. H., Pinsard, L. & Revcolevschi, A. (1998). *Phys. Rev. B*, **57**, R3189–R3192.

Rotiroti, N., Tamazyan, R., van Smaalen, S. & Mukovskii, Ya. (2005). *Acta Cryst.* C**61**, i83–i85.

Sage, M. H., Blake, G. R., Marquina, C. & Palstra, T. T. M. (2007). *Phys. Rev. B*, **76**, 195102.

Salamon, M. B. & Jaime, M. (2001). *Rev. Mod. Phys.* **73**, 583–628.

Salje, E. K. H., Carpenter, M. A., Malcherek, T. & Boffa Ballaran, T. (2000). *Eur. J. Mineral.* **12**, 503–519.

Salje, E. K. H., Graeme-Barber, A., Carpenter, M. A. & Bismayer, U. (1993). *Acta Cryst.* B**49**, 387–392.

Salje, E. K. H., Wruck, B. & Thomas, H. (1991). *Z. Phys. B Condens. Matter*, **82**, 399–404.

Sánchez, M. C., Subías, G., García, J. & Blasco, J. (2003). *Phys. Rev. Lett.* **90**, 045503.

Shannon, R. D. (1976). *Acta Cryst.* A**32**, 751–767.

Sondergeld, P., Schranz, W., Kityk, A. V., Carpenter, M. A. & Libowitzky, E. (2000). *Phase Transitions*, **71**, 189–203.

Sturge, M. D., Cohen, E., Van Uitert, L. G. & van Stapele, R. P. (1975). *Phys. Rev. B*, **11**, 4768–4779.

Swainson, I. P., Hammond, R. P., Cockcroft, J. K. & Weir, R. D. (2002). *Phys. Rev. B*, **66**, 174109.

Tachibana, M., Shimoyama, T., Kawaji, H., Atake, T. & Takayama-Muromachi, E. (2007). *Phys. Rev. B*, **75**, 144425.

Tarantino, S. C., Boffa Ballaran, T., Carpenter, M. A., Domeneghetti, M. C. & Tazzoli, V. (2002). *Eur. J. Mineral.* **14**, 537–547.

Tsvetkov, A. A., Mena, F. P., van Loosdrecht, P. H. M., van der Marel, D., Ren, Y., Nugroho, A. A., Menovsky, A. A., Elfimov, I. S. & Sawatzky, G. A. (2004). *Phys. Rev. B*, **69**, 075110.

Uehara, M. & Cheong, S.-W. (2000). *Europhys. Lett.* **52**, 674–680.

Uehara, M., Mori, S., Chen, C. H. & Cheong, S.-W. (1999). *Nature*, **399**, 560–563.

Ulrich, C., Khaliullin, G., Sirker, J., Reehuis, M., Ohl, S., Miyasaka, S., Tokura, Y. & Keimer, B. (2003). *Phys. Rev. Lett.* **91**, 257202.

Watanabe, S., Hidaka, M., Yoshizawa, H. & Wanklyn, B. M. (2006). *Phys. Status Solidi B*, **243**, 424–434.

Zhang, L., Israel, C., Biswas, A., Greene, R. L. & de Lozanne, A. (2002). *Science*, **298**, 805–807.

Zhou, J.-S. & Goodenough, J. B. (1999). *Phys. Rev. B*, **60**, R15002.

Zhou, J.-S. & Goodenough, J. B. (2005). *Phys. Rev. Lett.* **94**, 065501.

Zhou, J.-S. & Goodenough, J. B. (2006). *Phys. Rev. Lett.* **96**, 247202.

Zhou, J.-S., Goodenough, J. B., Yan, J.-Q. & Ren, Y. (2007). *Phys. Rev. Lett.* **99**, 156401.

Zubkov, V. G., Bazuev, G. V. & Shveikin, G. P. (1980). *Sov. Phys. Crystallogr.* **25**, 103–104.